"SILVER NANOWIRES: APPLICATION IN TRANSPARENT CONDUCTIVE FILMS (TCF) OF SOLAR CELLS"

Master's Degree in Renewable Energies, University of La Laguna

In cooperation with Fraunhofer Institut Solare Energiesysteme ISE

Esteban Rodríguez García

Tutor: Mario Mateo Jakas Iglesia
Physics Department

Index

1. Abstract

Silver nanowires (AgNW) becoming promising alternatives to indium tin oxide (ITO) in order to fabricate the transparent conductive films (TCF) that is often present in electronic devices and is an inevitable part of all photovoltaic solar cells. Motivated by this fact, this work shows the results of carrying out the synthesis of AgNW, its deposition on Si wafers together with ITO and the corresponding lamination processes to form solar modules. Furthermore, in order to observe the differences provided by nanowires, both, the electrical and optical properties of the solar cells coated only with ITO and with a combination of ITO and AgNW are measured. This comparison includes measurement of different Si wafer thicknesses as well as modification of the lamination structure on wafers of the same thickness with the coating formed by the combination of ITO and AgNW. The results in this paper show a positive influence of AgNW, as it has led to clear improvements of both the electrical and optical properties of the studied solar cells. This is a step forward on the route of substituing ITO for AgNW networks though, it must be said, stability and reproducibility of AgNW are problems that remain to be solved.

2. Introduction

A major challenge in the field of manufacturing highly efficient and flexible solar devices is the improvement of transparent conductive films (TCF).

Currently, the most widely used commercial material for transparent conductors is indium tin oxide (ITO) thin films since it provides an optimal tradeoff between resistance, transmittance and mechanical stability (high transmittance (80-90%) and low sheet resistance (10–100 Ω/sq.)) [1].

On the other hand, a dramatically increased demand in the touch panel industry, along with the fact that the main element of ITO is a rare metal (indium is about 75 wt %), will raise the price of this material [2].

Although ITO layers can be prepared at room temperature, they possess significantly low conductivity, and desirable sheet resistance can only be achieved with considerable film thickening [3].

As a consequence of the above, many efforts have been made to get alternatives to improve and substitute this material, such as metal oxides, graphene, conducting organic films, networks of carbon nanotubes, metal nanowires as well as metal mesh and hybrid nanostructures.

One of the most promising candidates is silver nanowires (AgNW) prepared via solution-based methods due to their excellent electrical properties such as low sheet resistance (Rs around 10,50 ohm/sq.) while maintaining a high transmittance (about 90%), which makes them suitable for scalable fabrication [4].

In contrast, individual AgNWs generally suffer from high contact resistance, wide surface roughness, poor adhesion to the substrate, etc. Despite the bright prospects, the main obstacle is the instability of AgNW [5]. Finally, connections between nanowires are superficial and that's not optimal for electric performance and durability of the device (because electromigration process could take place). Besides, another important problem with this kind of material is the lack of reproducibility of the structures generated from these processes.

Consequently, in order to solve not only the conductivity problems in ITO films, but also the stability issues shown by AgNW, a combination of both materials is presented as a possible solution towards obtaining a highly efficient TCF.

This work will focus on the study of optical properties of the cells both before and after the lamination process, attempting to evidence the effects of the combination of ITO and AgNW in those cells.

3. Silver Nanowires: an overview

3.1. Optoelectronic Properties and Performance

Electrical conductivity and optical transparency are the two key performance indicators, as the basic function of transparent conductive films is to conduct electricity and transmit light. Table 1 shows the optoelectronic requirements of this films for each target market [6]. It becomes difficult to improve them simultaneously.

Table 1. Requirements of transparent conductive films for different applications. Adapted from [6].

Applications	*Rs range [Ω sq−1]*	*T range [%]*
Resistive touch panel-touch side	300–500	86–90
Resistive touch panel-device side	200–500	88–90
OLED	10–50	>88
Transparent heater	2–10	>80
Solar cell	10–50	>88

3.1.1. Electrical conductivity

Electrical conductivity can be evaluated by the sheet resistance measure using the four-probe technique. Sheet resistance of AgNW electrodes could be influenced by the characteristics of individual nanowires, junctions between wires, distribution of nanowires on substrates and supporting materials around the nanowires. Characteristics of individual nanowires contain diameter, length and size distribution [6].

3.1.2. Optical transparency

Optical transmittance is measured with a spectrophotometer and for AgNWs remains almost unchanged in the visible range, being better than ITO in the IR region. Therefore, AgNWs are very useful in applications that require high transparency in the IR region. The optical transmittance is not only influenced by the dimensions of the nanowires, but also by their distribution on the substrates. Nanowires with smaller diameters show higher transmittance due to the lower proportion of photons that are scattered [7]. Thus, it can be affirmed that the optical transmittance is inversely proportional to the area density of the conducting nanowires [6]. Therefore, reflectance will be directly proportional to that area density.

3.1.3. Optoelectronic performance criteria

It is essential to evaluate the optoelectronic performance of transparent conductive films and compare them with established standards.

In this sense, TCF can be ranked by evaluating the figure of merit (FoM) from the ratio of DC and optical conductivities, σ OP/σ DC that relates transmission with sheet resistance (Rs), as it can be seen in the Eq. (1).

$$FoM = \frac{188{,}5}{R_S\left(\sqrt{\frac{1}{T_r}}-1\right)} \quad (1)$$

where Tr represents the optical transmittance at 550 nm and Rs is the sheet resistance.

Although the value of FoM helps to assess the trade-off between electrical conductivity and optical transparency, it is still unable to explain the relationship between nanowire characteristics and the optoelectronic properties of the film [4][6].

3.2. Material synthesis

As to the manufacture of high quality AgNW films, a lot of effort has been put on the low-cost controllable synthesis of high aspect ratio nanowires. Among the most developed methods are hydrothermal synthesis, wet chemical synthesis, template methods and the polyol process.

An encouraging method for the synthesis of nanowires is hydrothermal synthesis, which is capable of producing ultrafine nanowires with an average diameter of less than 15 nm and an aspect ratio of 1000 without any organic solvents at a relatively low temperature. However, the AgNWs synthesized by this method were not uniform and were obtained in low yield [6][8]**.**

The wet chemical method has the potential to obtain high purity products, but it is difficult to transfer and assemble them [9].

Template-based methods have been widely used for the first time to generate AgNWs and can be classified as hard template methods and soft templates. Their main advantage is that prepared AgNWs can be synthesized in a very controlled way [8].

However, hard template methods are expensive and complex due to preparation and elimination of templates [6]. In addition, this purification process can damage the nanowires, especially those with a high aspect ratio [8].

To deal with the drawbacks of hard template methods, efforts have focused on soft template-based strategies. These templates have the fundamental characteristic of being able to dissolve into solution. However, products synthesized by this method are often full of low yields, irregular morphology and low aspect ratios [8].

Another interesting method resorts to UV irradiation. A photo-reduction process in which Ag^{+} serves as a precursor solution, and a suitable surfactant is added as a protective agent to induce photo-reduction of silver nitrate ($AgNO_3$), all through a photo-decomposition step under UV radiation conditions. The following Eq. (2) describes the mechanism of formation of Ag nanostructures:

$$2AgNO_3 \xrightarrow{hv} 2Ag + 2NO_2 \uparrow + O_2 \uparrow \qquad (2)$$

Among the various ways of synthesizing AgNWs, the polyol method has certain advantages in terms of cost and mass production, and is currently the standard method for preparing AgNWs [10].

AgNWs were obtained from the reduction of $AgNO_3$ in presence of polyvinylpyrrolidone (PVP) seeds. Ethylene glycol (EG) is generally used as a solvent and reducing agent, PVP is used as a coating and template agent, and $AgNO_3$ is used as an Ag source [10]. Different salts such as NaCl and $CuCl_2$ are used to reduce the reaction time and improve synthesis. High molar weight of PVP, proper amount of chloride, high injection rate of $AgNO_3$ and PVP, low temperature reaction and low stirring rate are the best parameters to synthesize nanowires with a high aspect ratio [6].

3.3. Fabrication process

Developing a low cost, high performance, large area, reliable and simple technique is critical when forming AgNW networks.

Many solution-processed coating methods have been proposed, being the three most relevant the spin coating method, the inkjet print method and the roll-to-roll method.

3.3.1. Spin coating method

Spin coating method has three steps: dosing, high speed rotation and film volatilization. Concentration and viscosity are key parameters for controlling film thickness. Among them, rotation speed has a great influence on thickness and yield. Higher speed gives thinner film, lower speed gives thicker film [11]. However, when rotation speed is too high, film breaks easily, while if speed is too low, the AgNW of ink is susceptible to aggregate, resulting in unequal distribution of them.

A higher rotation speed results in lower AgNW density, higher transmittance and lower electrical conductivity. Therefore, adjusting angular rotation speed is very important for the performance of the film (Figure 1).

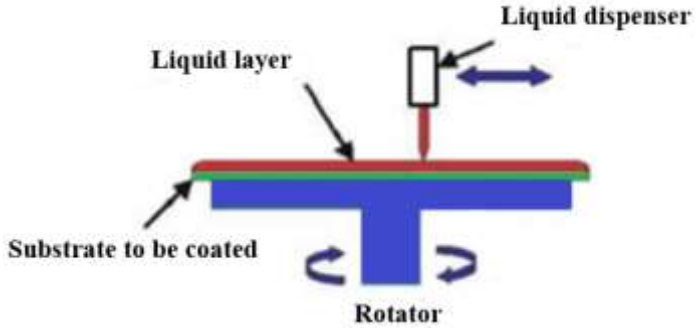

Figure 1. Schematic of spin coating process. Adapted from [12].

3.3.2. Inkjet print method

Inkjet printing is a technique that precisely deposits functional materials onto the corresponding parts of a substrate by means of contactless, pressureless and no-print operation (Figure 2). This technique is based on dispersion of a conductive ink by dissolving a conductive material such as AgNW in a solvent, and then expelling the ink under the control of a computer that forms a dot pattern [13]. Currently, inkjet printing

technology is divided into continuous inkjet and drop-on-demand inkjet. Today, drop-by-drop inkjet printing technology is commonly used to prepare AgNW's transparent conductive electrodes (TCE) at a lower cost and in a flexible way. Compared to the spin-coating method, inkjet printing is suitable for automation and high-resolution pattern making. Direct access to the TCE with pattern simplifies the process and reduces cost, and further promotes the application of AgNW's TCE [10].

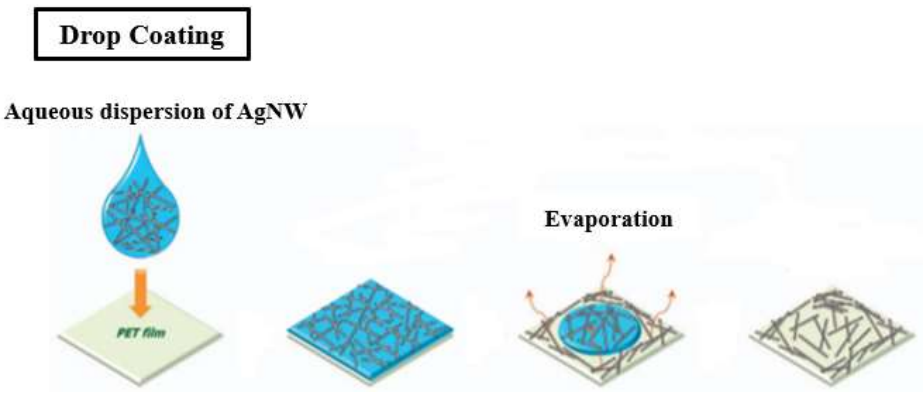

Figure 2. AgNW networking process on polyethylene terephthalate (PET) film by drop coating. Adapted from [14].

3.3.3. Roll-to-Roll process

Currently, the process most likely to achieve mass production is the roll-to-roll method (RTR). This is a new process for producing an electronic device by pressing a flexible substrate such as polymer film onto a roll of paper (Figure 3). This process allows electronic ink to be applied to a flexible substrate a few meters wide and 50 meters long [15], resulting in a significant reduction in production cost.

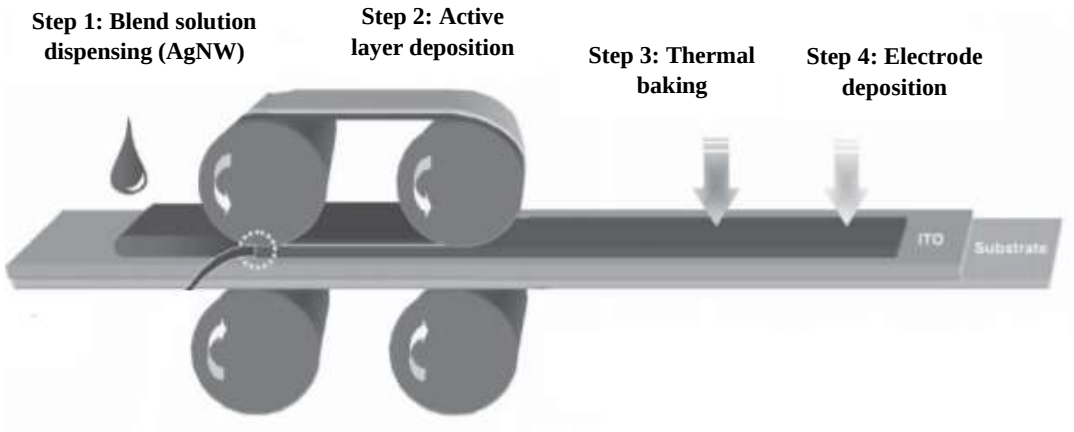

Figure 3. Schematic diagram of a roll-to-roll process. Adapted from [16].

4. Lamination process

4.1. Introduction

Lamination is a crucial step in the manufacturing process of photovoltaic modules to guarantee optimum performance of the solar modules on the outside.

Encapsulation consists of substrate - encapsulant - cells - encapsulant - cover (Figure 4).

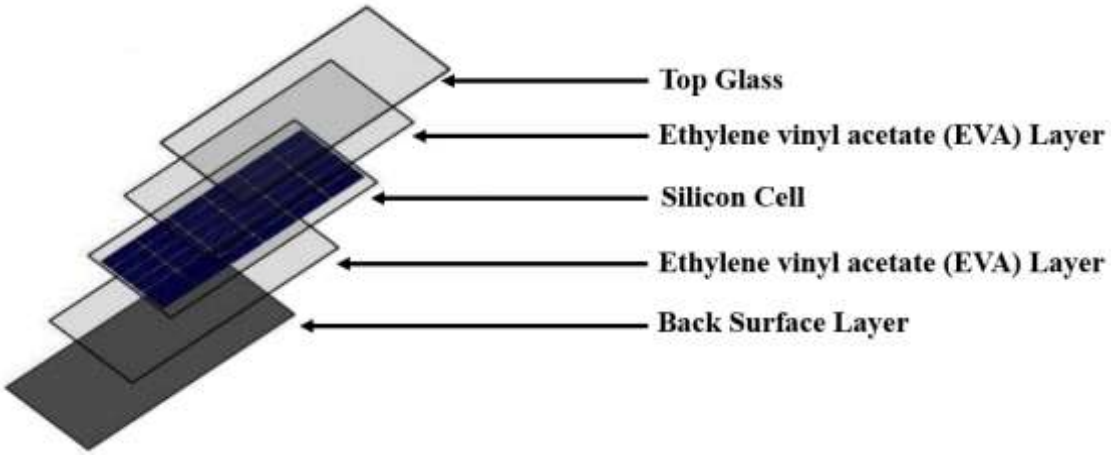

Figure 4. Several components of a photovoltaic module. Adapted from [17].

Lamination process consists of creating a vacuum to extract any gases that may be present in the photovoltaic module and applying pressure to make sure that all the materials are bonded together (Figure 5). Proper lamination should maintain solar cells in good condition for at least 25 years.

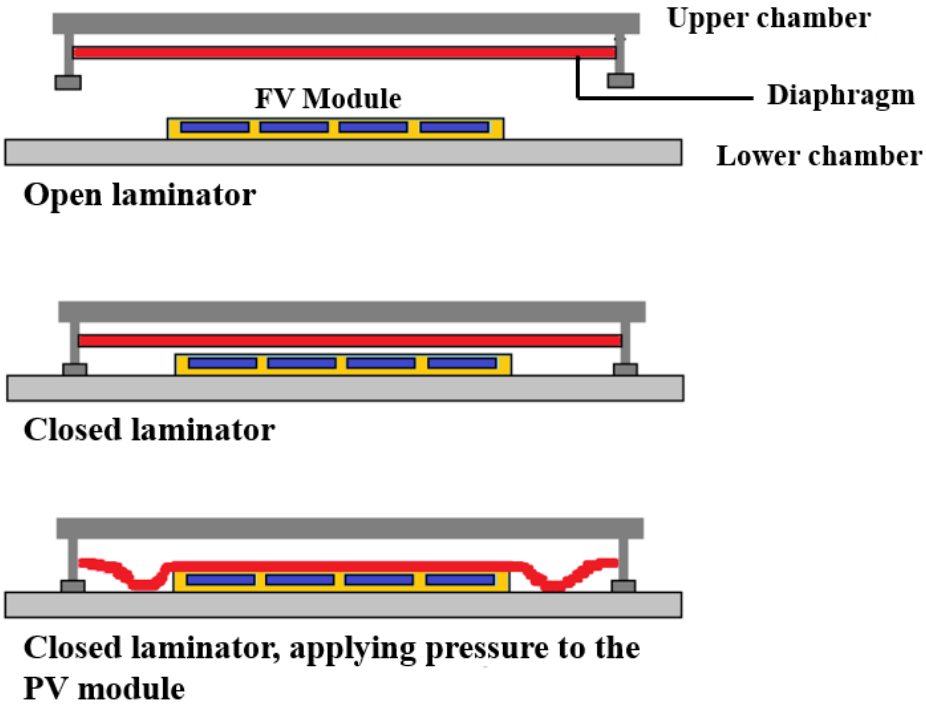

Figure 5. Lamination process.

4.2. Description of the laminator

There is a cover on the unit that locks the edges hermetically. This cover has an internal chamber and a diaphragm that separates this chamber (upper chamber) from the chamber containing the module (lower chamber) (Figure 6).

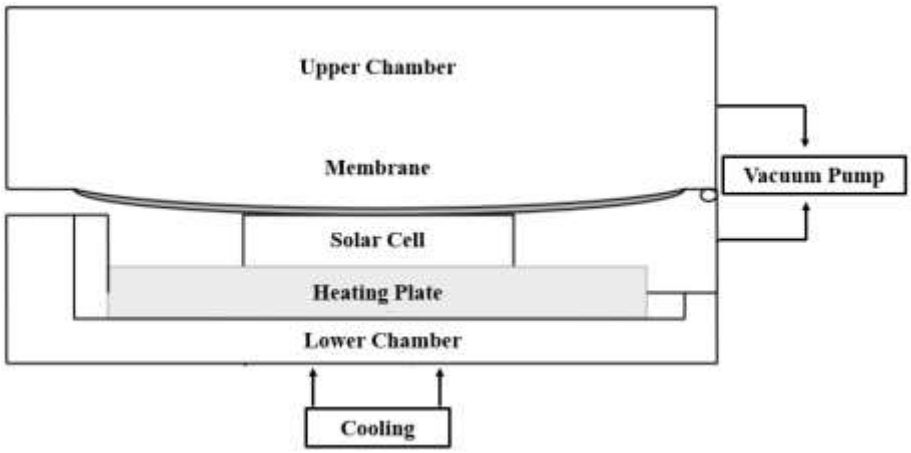

Figure 6. Lamination machine scheme. Adapted from [18].

Both chambers can be evacuated independently. Sample is introduced into the lower chamber, between two Teflon sheets. This configuration allows the module to be under vacuum while mechanical pressure is applied to it.

To heat the sample, the unit is equipped with an aluminium plate that is heated by three resistances. Figure 7 shows the different parts of the laminator:

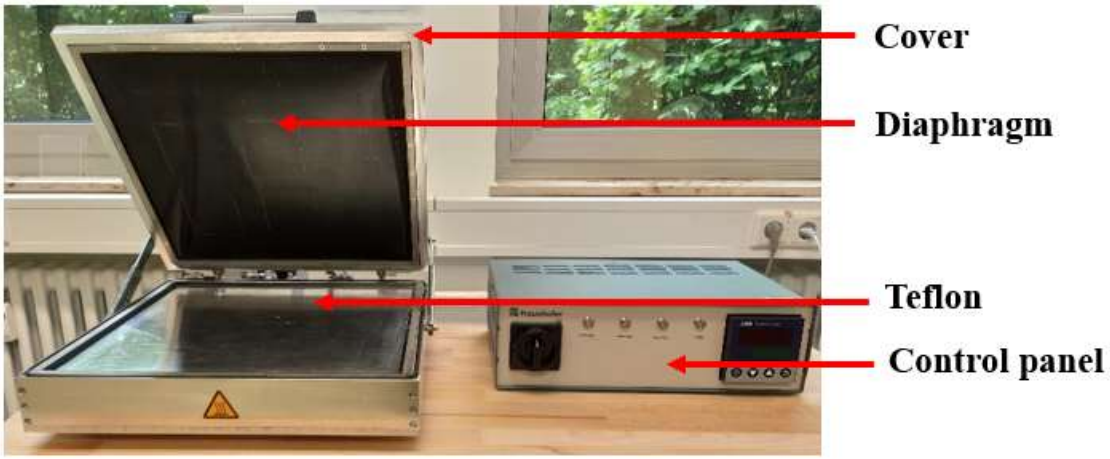

Figure 7. Parts of a laminator.

4.3. Laminator's operation

At first, the laminator is switched on, sample is inserted between the two teflon sheets, machine is locked and the desired formula is added using the touch screen with the appropriate temperature, pressure and time parameters. Once this is made, the laminator

will be heated until it reaches the desired temperature. At this point, the lamination process begins, as shown in Figure 8.

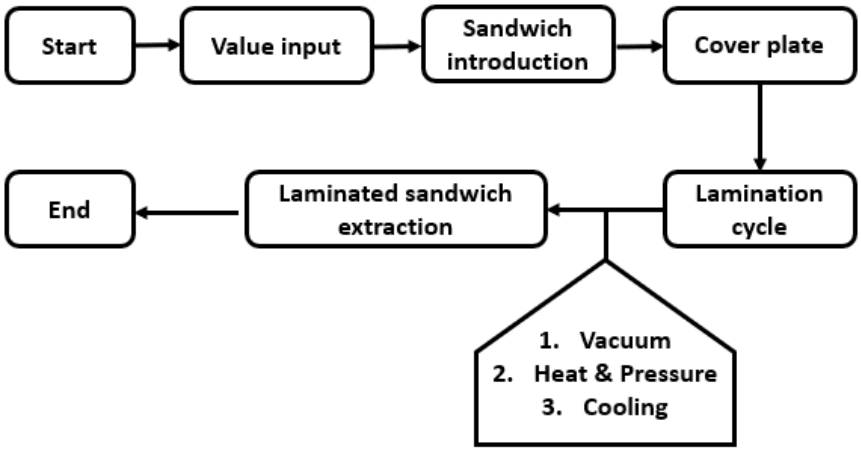

Figure 8. Description of the laminator's operation.

The lamination process can be divided into three stages (Figure 9):

1) A vacuum is created in both chambers (0-10 mB), with the aim of extracting air, humidity or other gases that may be found between the layers of the module.
2) The upper chamber is filled with compressed air so that the membrane pushes the material to be laminated. Meanwhile, curing of the EVA takes place. Plastic acquires elastomer properties.
3) A vacuum is created in the upper chamber and the vacuum is broken in the lower one, allowing the chamber to be opened and the lamination process to be completed.

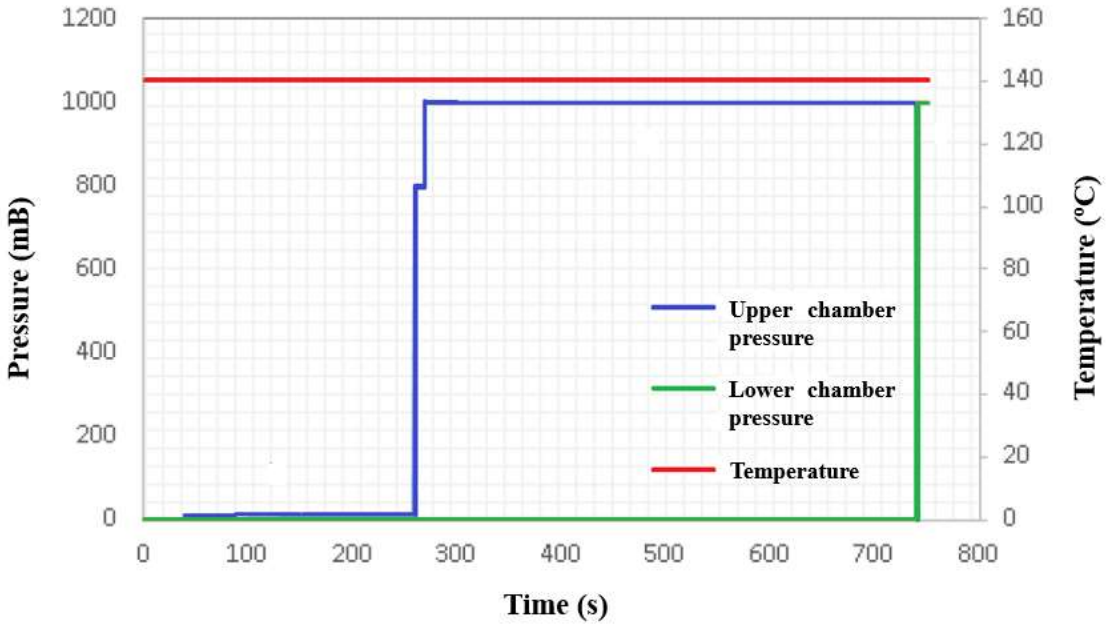

Figure 9. Pressure and temperature during the lamination process.

5. Experimental part

5.1. Measurement technology and characterization methods

The following section describes the measuring equipment used: for the electrical properties it was used the Fakir measuring station developed by the Fraunhofer ISE, while for the measurement of the optical properties a spectrophotometer is used. In addition, a precision balance, a thermocouple for the heating furnace and a microscope for visual inspection of the nanowires and their properties were used in the production process.

5.1.1. Spectrophotometer

Optical measurement values are recorded with the assistance of Varian's "Cary 500" photo spectrometer (Figure 10). This instrument is capable of measuring transmission and reflection and evaluating them by means of software.

Figure 10. Spectrophotometer Varian Cary 500.

The functionality of the photo spectrophotometer is as follows (Figure 11):

A light beam is generated by a tungsten wire halogen lamp (for the infrared wavelength range) and a deuterium lamp (for the ultraviolet wavelength range). Light enters a monochromator which filters out a certain spectral wavelength. The monochromatic light beam is then divided by a beam splitter into a measuring and a reference beam. These pass through deflecting mirrors to the integrating sphere. It consists of two supports and a sensor. The intensity I, of the light, the reference beam and the measurement beam, is now alternately detected by the sensor. Measured data are transmitted to a computer which evaluates them by transmission or reflection.

If transmission is to be measured, a so-called white stone must be fixed in the sample holder 2. This stone reflects incident light, which has passed the sample before, back to the integrating sphere, which in turn reflects the light back to the sensor. Thus, total light that has passed through the sample is measured and the measured value for transmission of the respective sample is obtained.

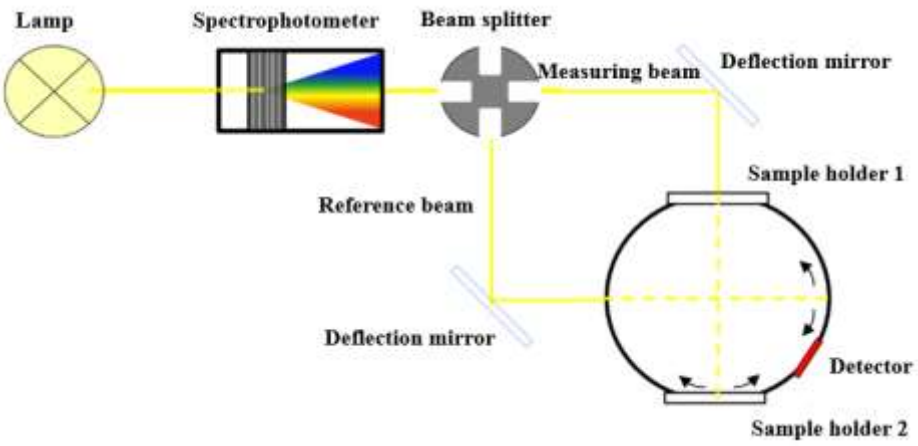

Figure 11. Mode of operation of the spectrophotometer. Adapted from [19].

5.1.2. Fakir measuring station

This measuring station makes use of the principle of the four-point method (Figure 12):

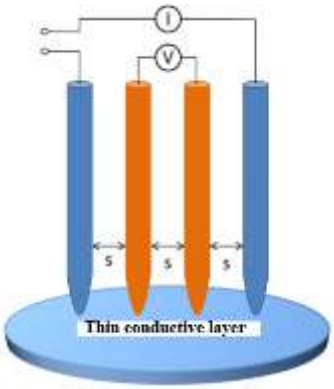

Figure 12. Four-point method. Adapted from [19].

A defined current flows over the two outer needles (blue). The distances between needles are also known. Current flowing between the outer needles generates a voltage drop U. This is measured through the inner needles (orange) and according to $R_{sh} = \frac{U}{I}$ the resistance per area can be calculated. Fakir measuring station (Figure 13) can apply this method over an entire area.

Figure 13. Fakir measuring station.

5.1.3. Microscope

An Olympus microscope, model AX70, was used for microscopy (Figure 14). It has five objectives with 5x, 10x, 20x, 50x and 100x magnification. In addition, binocular of the microscope has a 10x magnification, so that the samples can be seen at a maximum magnification of 1000x. Microscope also has a camera connection so that it is possible to take pictures of the microscopic samples.

Figure 14. Microscope Olympus AX70.

5.1.4. Precision balance

Precision balance (Figure 15) was used in the silver nanowire synthesis. Specified measurement accuracy is 1 mg, maximum load 150 g. Weighing paper by Carl Roth was also used.

Figure 15. Precision balance with draft shield.

5.2. Process Technology

5.2.1. Oven

Carbolite oven is used (Figure 16). This furnace is regulated very quickly and also with great precision, so that the actual temperature soon returns to the target temperature after the sample has been introduced or individual samples have been taken.

Figure 16. Carbolite oven.

5.2.2. Magnetic stirrer

A Phoenix magnetic stirrer, model RSM 10HS, was used to mix the solutions (Figure 17). A magnetic stirring rod is placed in the solution cup and placed on the plate.

Figure 17. Magnetic stirrer, glass with stirring rod on top.

5.2.3. Ultrasonic bath

Ultrasonic bath is made by Sonorex, model Super RK 512H (Figure 18). It is used to dissolve silver nitrate in ethylene glycol and to mix silver nanowire solutions homogeneously to prevent clustering.

Figure 18. Ultrasonic bath.

5.3. Synthesis of silver nanowires (AgNW)

Silver nanowires are synthesized by the so-called polyol method. A solution of ethylene glycol (EG), polyvinylpyrrolidone (PVP) and silver nitrate ($AgNO_3$) is heated to 170°C for about 120 minutes. This produces silver ions (Ag^+), which grow on wires through homogeneous nucleation. The exact manufacturing process is based on the experiments carried out by the Fraunhofer Institute team and is as follows:

Three initial solutions are produced:

- Copper (II) chloride solution:

Copper (II) chloride serves as an accelerator of the reaction and is only needed in small quantities. Therefore, an ethylene glycol solution is prepared in which the concentration of copper (II) chloride is 1 mM.

- PVP solution:

Polyvinylpyrrolidone is also dissolved in ethylene glycol. The PVP should be PVP K-90 (molar mass Mw = 360,000 g/mol). The higher the molar mass, the longer the PVP chains. PVP is very difficult to dissolve and should be prepared about 3 days in advance.

- Silver nitrate solution:

To prepare this solution, 120 mg silver nitrate is dissolved in 7,5 ml ethylene glycol. Silver nitrate is also poorly soluble and therefore should be placed in an ultrasonic bath for about 10 minutes. After the ultrasonic bath, a change in colour is observed (from transparent to yellowish or even tanned (Figure 19)).

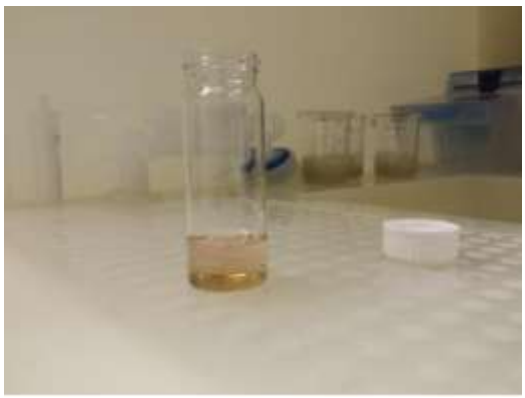

Figure 19. Silver nitrate dissolved in ethylene glycol after an ultrasonic bath.

First, ethylene glycol ($HOCH_2CH_2OH$) is reduced to acetaldehyde (CH_3CHO) and water (H_2O) Eq. (3). Then silver ions react with acetaldehyde to form diacetyl ($CH_3CO\text{-}OCCH_3$), pure silver (Ag) and hydrogen ions (H^+) Eq. (4).

$$2\,HOCH_2CH_2OH \rightarrow 2\,CH_3CHO + H_2O \quad (3)$$

$$2\,Ag^+ + 2\,CH_3CHO \rightarrow CH_3CO - OCCH_3 + 2Ag + 2H^+ \quad (4)$$

Now silver nitrate solution and PVP solution are added alternately and dropwise to the copper (II) chloride solution. Using the pipette, 500 µl were each pipetted and then slowly dropped into the copper (II) chloride solution, which was kept under constant agitation by the magnetic stirring rod (300 rpm). In this way, a homogeneous mixture was achieved. The beaker containing the solution is now covered with a watch glass and placed in the oven at 170°C for 120 minutes.

A change in colour occurs, from yellowish (formation of silver ions) to greyish (joining of the silver wires) (Figure 20).

Figure 20. Color changes in the oven A to F (0 to 120 minutes).

Silver nanowires (Figure 21) have a diameter of approximately 20 to 40 nm and a length of 40 to 200 µm. Together, these nanowires form a grid similar to that of a structured metal mesh.

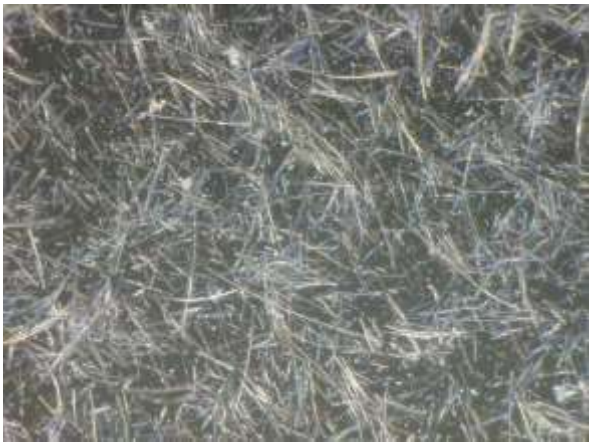

Figure 21. Microscopic picture of the silver nanowire mesh (1000x zoom).

5.4. Deposition of silver nanowires (AgNW)

5.4.1. Mayer-Rod's process

This is a much more manual process than those seen in previous sections, since the experiments carried out do not require the application of a method with commercial range.

In this process a spiral rod is used to distribute the dispersion uniformly on the substrate (Figure 22). A Mayer-Rod is basically a steel rod around which a wire is coiled.

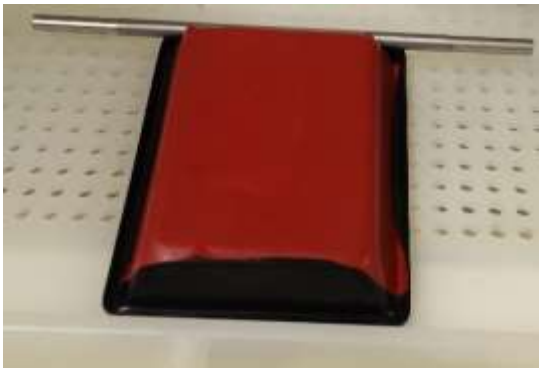

Figure 22. Mayer-Rod's rod in front of a gummed surface. The gum coating prevents slipping.

Depending on the thickness of the wire, results in a defined layer thickness. Dispersion is applied to the edge of the sample, and spiral with coiled wire is also applied there. Rod is drawn once over the sample. It is important to ensure constant speed and pressure. This solution is distributed uniformly, excess amounts are scraped off at the other end and remaining isopropanol in the solution is evaporated (Figure 23).

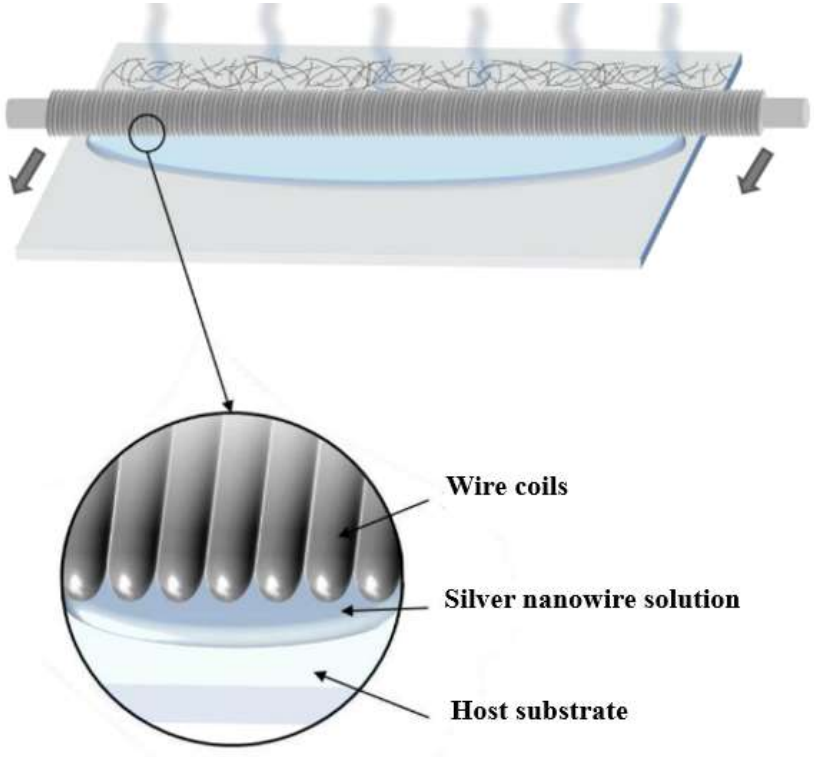

Figure 23. The Mayer-Rod process. Adapted from [19].

5.5. Coating of the Si wafer with indium tin oxide (ITO)

ITO deposition is performed by ion sputtering on the surface of the Si wafer, using a high vacuum chamber (Figure 24).

Figure 24. Pfeiffer Balzers PLS 500 high-vacuum test chamber.

5.6. Preparation of the different layers for the lamination process

At the same time as the solar cell is prepared, both with the ITO and AgNW coating, it is necessary to prepare the remaining component layers of the lamination process.

The order in which the lamination process is placed is as follows:

Glass → EVA → Si Wafer → EVA → Back Surface Layer

5.6.1. Tempered glass cutting

Its function as a front cover, is to protect the cell from impacts and different atmospheric agents.

- Measurements are taken from the silicon wafer. The standard is usually 12,5 x 12,5 cm.
- Handle moves the y-axis; button handle moves the x-axis (Figure 25).

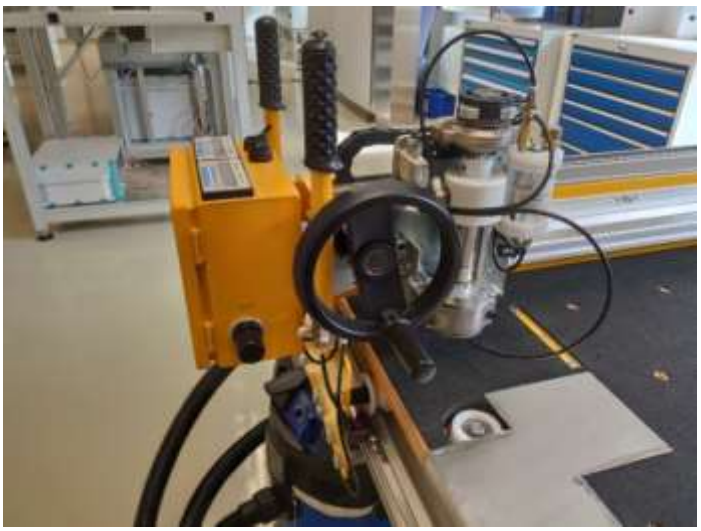

Figure 25. Machine used to cut the glass.

- 2mm is left uncut for safety.
- A clamp allows the glass piece to be extracted.
- Profiles are smoothed to eliminate the possibility of cutting with the glass.

5.6.2. Encapsulating material cutting (EVA)

Its function is to seal the cells with both the front and back covers, as well as to maximize optical coupling and protect the cells from moisture.

- Cut glass is used as a reference.
- Cuts are made with a cutter.
- It is done in a duplicate procedure.

5.6.3. Back-surface layer cutting

It has the same purposes as the front cover, as well as acting as an electrical insulator.

- The glass is used as a reference, but this time with a certain amount of clearance to prevent EVA residues from overflowing.

6. Results and discussions

Experiment carried out consists of the deposition of a layer of AgNW in combination with a double layer, front and back, of ITO on a silicon wafer.

Firstly, electrical measurements of the sheet resistance are carried out for all the wafers, comparing values obtained only with ITO layers and values obtained from the combination of ITO and AgNW.

Main experiment is based on comparing the reflectance of wafer with ITO only and wafer with the addition of AgNW layer, both before and after the cell lamination process.

6 Si wafers of different thicknesses (160 μm, 200 μm and 250 μm) are coated, first with AgNW and then with the double layer of ITO. Each wafer thickness is replicated and compared to an ITO-only coated wafer (Figure 26). However, each replication is not exactly the same, as one of them will be subjected to a standard lamination process, while the other will not have a back-surface layer, but another glass plate, in order to observe any potential differences.

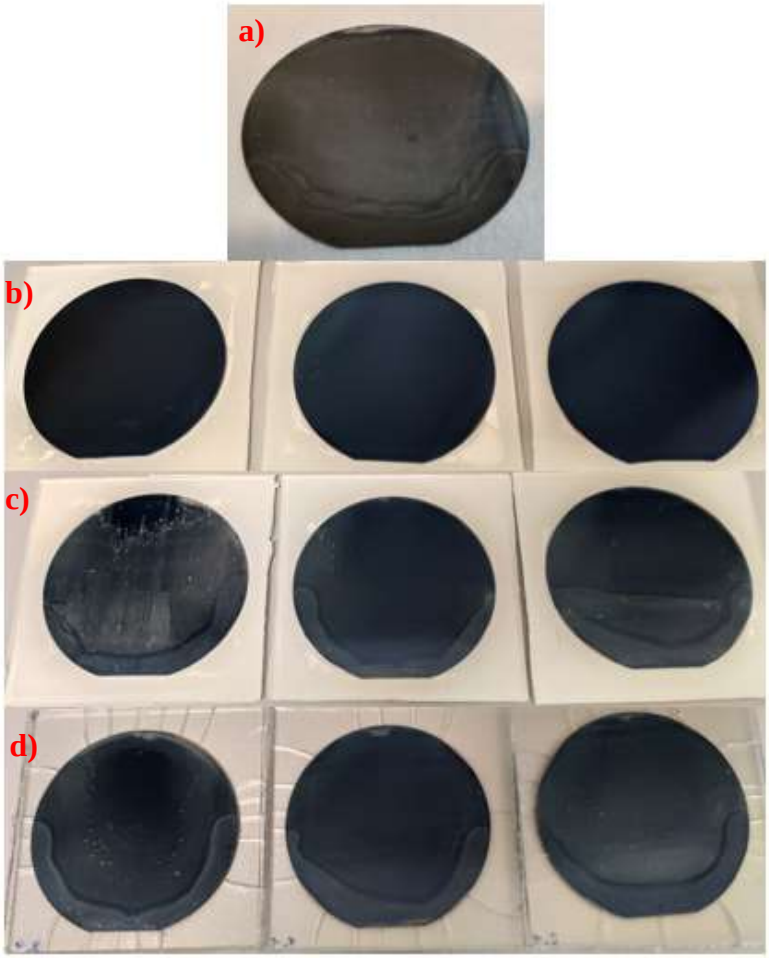

Figure 26. a) ITO and AgNW coated Si wafer without lamination. b) ITO coated Si wafers only after the lamination process. c) ITO and AgNW coated Si wafers after the lamination process. d) ITO and AgNW coated Si wafers after the lamination process without back surface layer, just only with a glass-glass lamination process.

Previous studies have shown that smaller diameter nanowires show lower reflectance due to the smaller proportion of photons dispersed [7]. In addition, optical reflectance is directly proportional to nanowire area density [20]. Thus, a higher density, together with large diameters will make the optical conditions worse.

However, the electrical properties could be affected. On the one hand, fewer wires are needed for films with longer nanowires to make a conductive path through a given space, which leads to fewer junctions and lower resistance. On the other hand, an increase in density of the nanowires results in a decrease of sheet resistance [21][22]. In other words, small lengths and low densities are optimal conditions for low reflectance values, while large wire lengths and high densities lead to better sheet resistance values. For all this it is necessary to reach a trade-off that allows good values in both fundamental properties for the constitution of a solar cell.

6.1. Electrical measurements

Measures were carried out with the assistance of the Fakir measuring station and results obtained for all samples are shown in the following table:

Table 2. Sheet resistance measures for all the samples.

Wafer thickness	Si wafer coating	R_{sheet}(Ω/sq.)
160 µm	ITO	22,31
	ITO + AgNW 1	13,12
	ITO + AgNW 2	13,22
200 µm	ITO	21,74
	ITO + AgNW 3	12,4
	ITO + AgNW 4	12,26
250 µm	ITO	20,95
	ITO + AgNW 5	11,17
	ITO + AgNW 6	10,53

As can be seen, values obtained after the application of AgNW have improved significantly. These results were to be expected since the estimated sheet resistances for coating with ITO alone are between 10-100 ohm/sq. [1], while for AgNW these values are much more constant at 10,5 ohm/sq. [4].

6.2. Optical measurements

Transmittance values for glasses and reflectance values for all silicon wafers under study were measured. These last ones, both before and after the lamination process.

These measurements were carried out with the assistance of Varian Cary 500 spectrophotometer in the 300-1200 nm wavelength range, taking a large part of the sun's electromagnetic range (avoiding the ultraviolet c region, which barely reaches the atmosphere, and the higher infrared region, above 1200 nm, which does not represent a large percentage of the total use, so it is possible to limit the spectrum).

First of all, transmittances of the 6 glasses that will be part of each of the laminated solar cells are measured, to check that there is no significant alteration in them (Figure 27). In

order to perform this study, there is no anomalous values in the whole of the glasses. They all exhibit at least the same behaviour: a clear downward trend from 400 nm, with peaks at 420 nm (around 94 % transmittance) and fairly high values in the infrared area.

The following are the reflectance results obtained for all wafers of every thicknesses under study (Figure 28, 29 and 30).

Figures show the reflectance for a certain wafer thickness before the lamination process in a) and a comparison between before and after lamination in b).

Section a) shows 6 curves of reflectance; front (FS) and back (BS) layers of the ITO-only coated cell and the two ITO and AgNW-coated replicas.

As can be seen, both sides of the ITO wafer and the rear sides of the combined ITO and AgNW show the same behaviour, as in all these cases the reflectance of a single ITO layer is being studied. Results change with the front layers of the ITO and AgNW samples, as the presence of the nanowires makes the values obtained worse, especially in the central range between 600 and 1000 nm. Similarly, curves for both AgNW replicates should be the same, but this condition is only met for the 160 µm wafer thickness and not for the following 200 and 250 µm. This is probably due to the lack of uniformity in the deposition method as it is a manual deposition.

On the other hand, section b) compares front layers of wafers with ITO only and the two replicas with ITO and AgNW with the same layers but after the lamination process. However, there is now a distinction between the two replicas of each wafer thickness. In order to find differences and make comparisons, the lamination process is carried out with the standard structure for one of them (Glass-EVA-Wafer-EVA-Back-Surface Layer) called G-B in the figures and with a modified structure for the other one (Glass-EVA-Wafer-EVA-Glass) called G-G.

The first comparison is made between cell with ITO and replica with Back Surface layer. In this case, a small improvement of the ITO with AgNW is observed, around 3-4 % around the peak of maximum reflectance at 400 nm. In addition, in the intermediate range between 600 and 1000 nm, possible differences due to non-uniformity in deposition processes for the two replicates are eliminated and the degradation compared to the laminated cell with ITO alone is reduced (from 5-12% to 2-5%). In the last range, between 1000 and 1200 nm, reflectance values increase significantly, both for the ITO-only cell and for the AgNW replica with back-surface layer, although the last one to a lower degree. However, the replica with another glass replacing back-surface layer shows a clear improvement (25-30% reflectance versus 45-50% for the other two cells). A big difference in this replica does not concern the intrinsic properties of the AgNW, but the differences in the back-surface layer and its reflectance.

It is worth adding that there are no remarkable differences in results obtained in relation to the thickness of wafers. Given the results, slightly more extreme values must be reached, both above and below, for this parameter to have an impact.

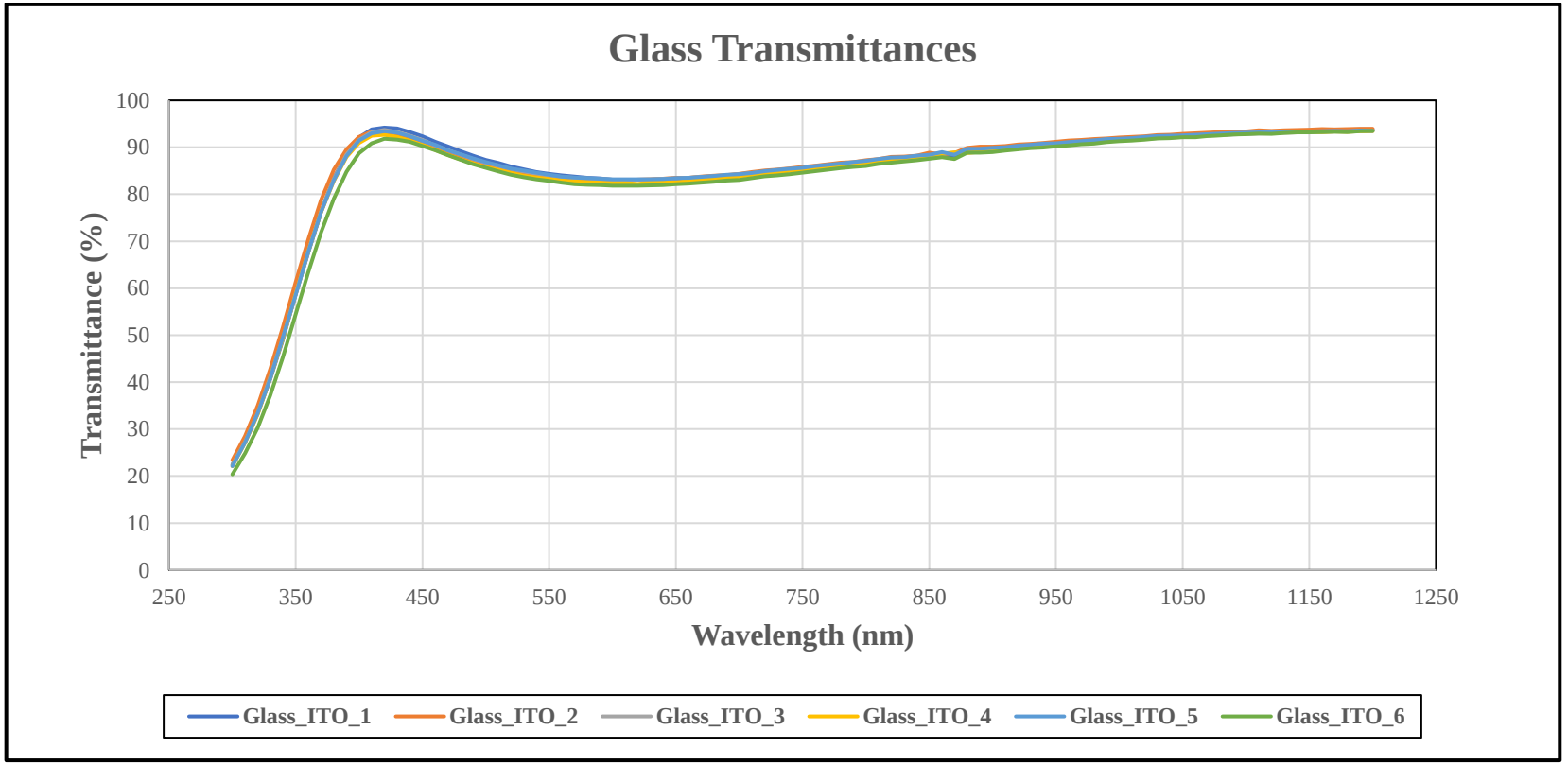

Figure 27. Glass transmittance values.

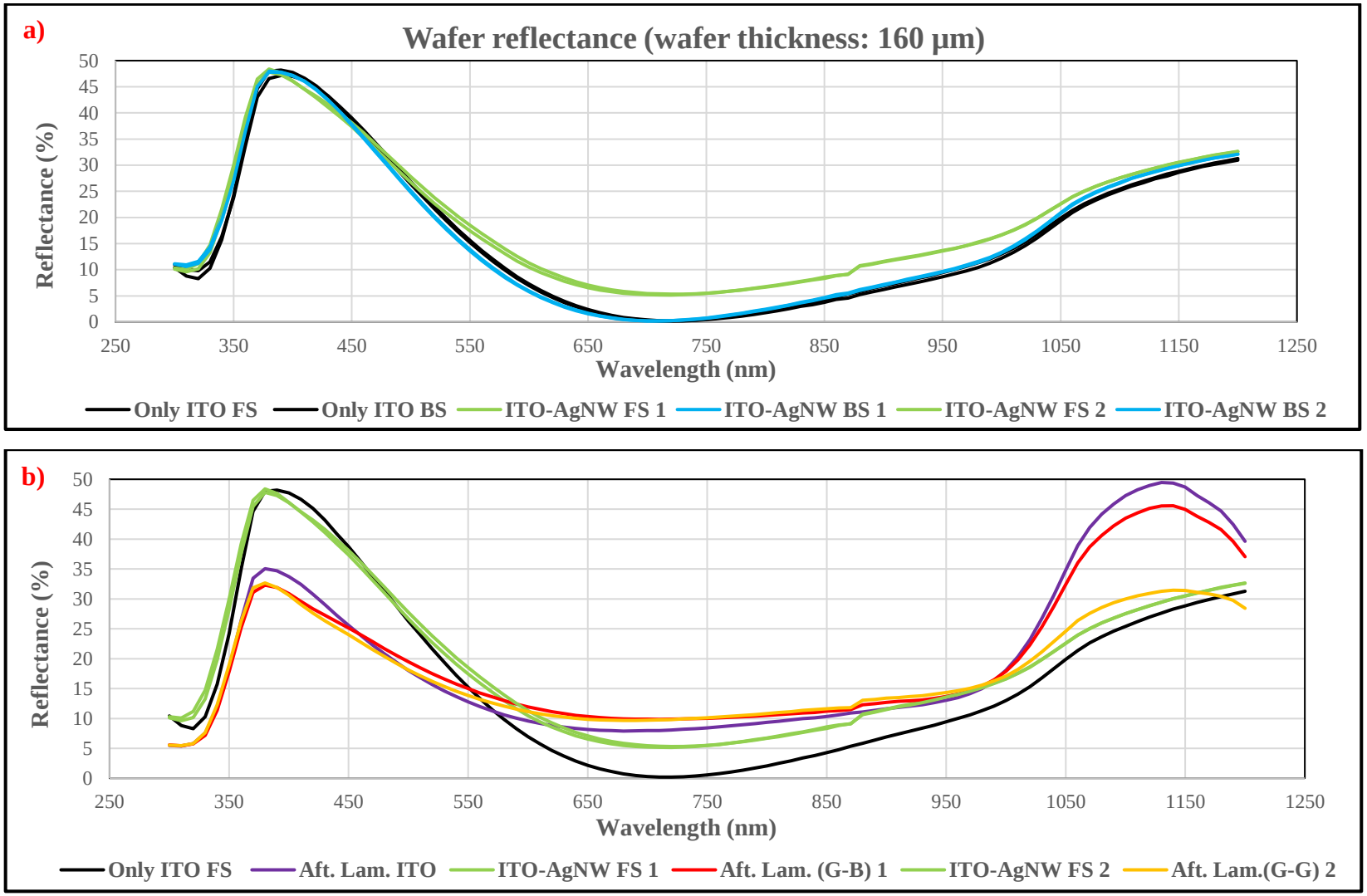

Figure 28. Reflectance of Si wafers with a thickness of 160 µm a) before the lamination process b) before and after the lamination process.

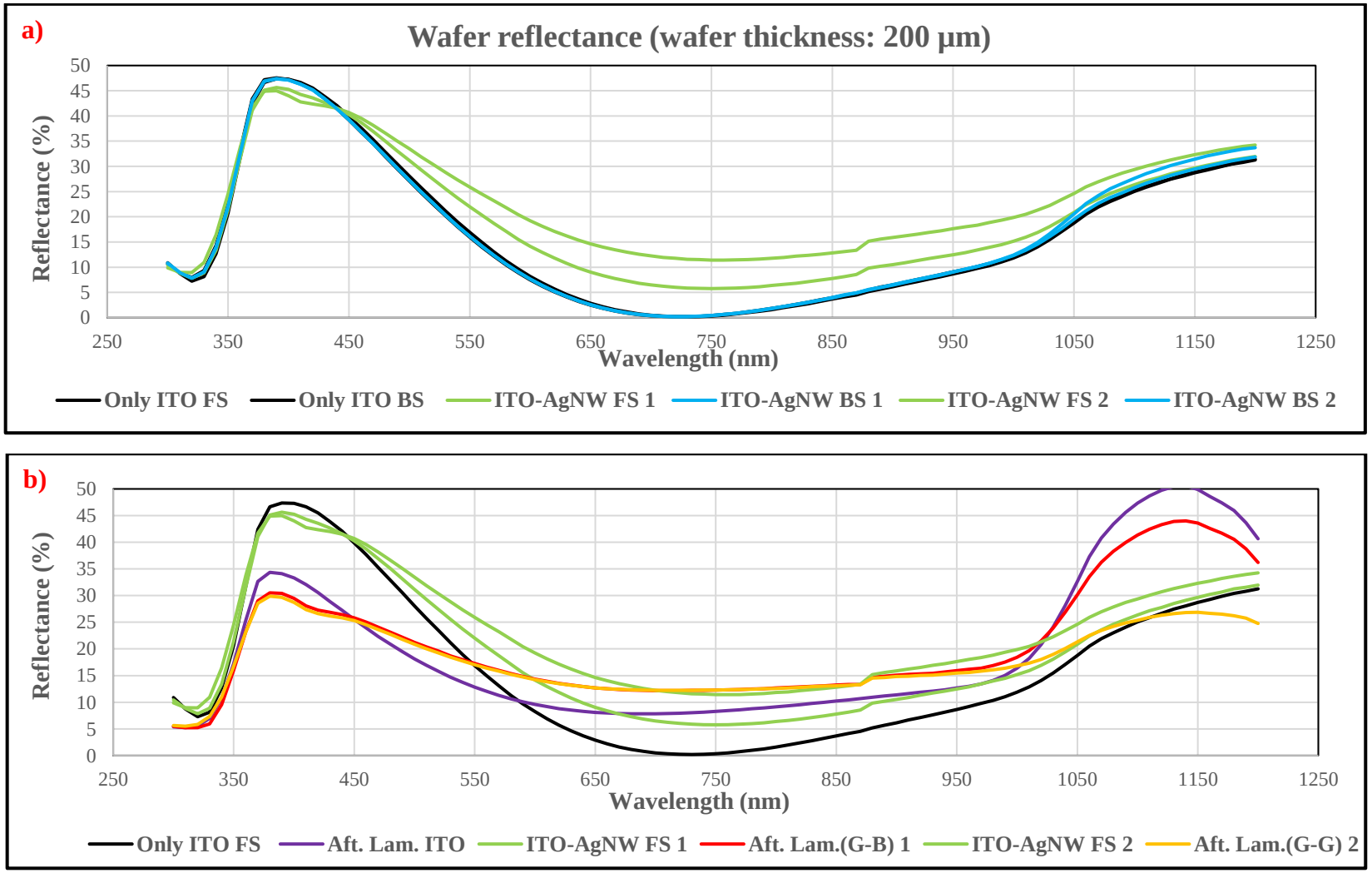

Figure 29. Reflectance of Si wafers with a thickness of 200 µm a) before the lamination process b) before and after the lamination process.

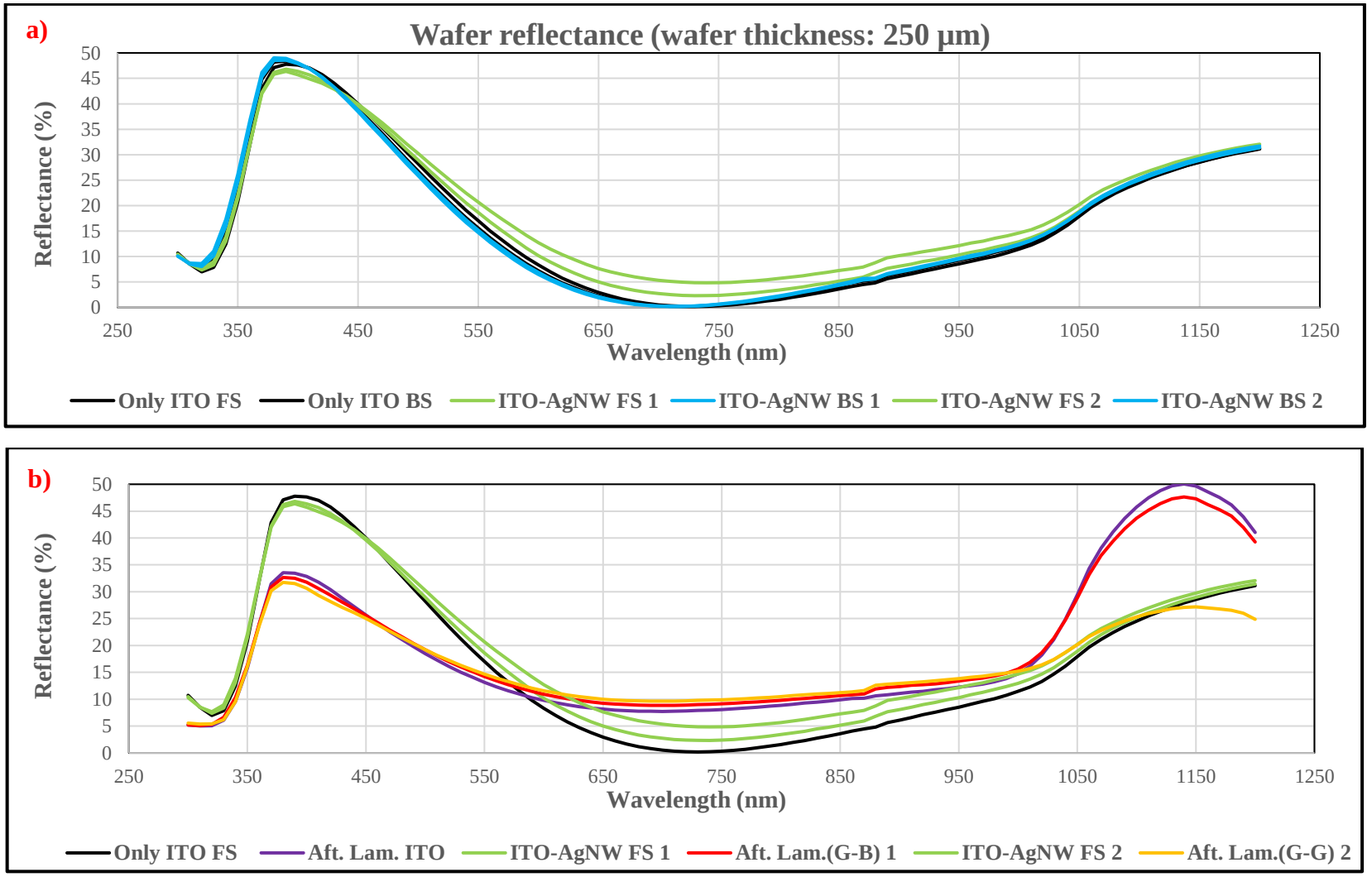

Figure 30. Reflectance of Si wafers with a thickness of 250 µm a) before the lamination process b) before and after the lamination process.

7. Conclusions

With the purpose of studying the benefits that silver nanowires (AgNW) may have on the solar cells, AgNW are synthesized and deposited into Indium-Tin-Oxide (ITO)-coated solar cells and the electrical and optical properties of such (AgNW-ITO) cells are studied. Results in this paper show that the sheet resistance (R_s) exhibit clear improvements with the addition of AgNW. It is found that R_s of approximately 20 Ohm/sq. for samples coated only with ITO reduces to values ranging between 11 and 13 Ohm/sq. for (AgNW-ITO)-cells.

On the optical side, it is observed that spectral reflectance shows a small improvements in the beginning of the ultraviolet and part of the visible range (between 300 and 600 nm), while in the rest of the visible and the first part of near infrared (between 600 and 1000 nm) reflectance increases to a certain level with presence of AgNW. It should be added that after the lamination process, the difference in reflectance towards higher and, therefore, worse values produced by the AgNW in the middle regions of the spectrum, decreases compared to non-AgNW samples, resulting in a reduction of the negative contribution of AgNW in these areas.

Finally, between 1000 and 1200 nm reflectance decreases again, with replicas replacing the back-surface layer with another glass layer showing the best values (25-30% reflectance versus 45-50% for the replica with a standard lamination). Considering that the solar maximum is above 500 nm, improvements compensate for the small increases in some of the commented areas.

Overall, it can be concluded that AgNW deposition contributes to the enhancement of solar cell properties, to the point that coatings based only on AgNW appear to be a plausible approach to manufacturing solar cells. Still challenges are ahead, namely the stability and reproducibility of the AgNW though important, as it may be figured out, these topics that were scarcely covered in this paper.

8. Acknowledgements

This work was supported by the German entity Fraunhofer Institut Solare Energiesysteme ISE, where the whole experimental part was carried out. Within the institution, I would like to give special thanks to Christian Roters, who has been involved with great passion and total interest in the proper development of this work. Likewise, I would like to acknowledge the centre's director Dr. Dietmar Borchert and Dr. Stefan Hohage for their support and continuous assistance.

In a different area, I would like to express my gratitude to my work tutor, Mario Mateo Jakas Iglesia, for his total disposition and willingness to provide any kind of help needed.

Finally, I would like to mention my colleague from Germany, Mario Sebastián Pinto Miranda, with whom I have shared a large part of the experimental procedure in the laboratory and of living together in a country that is completely new for both of us.

9. References

[1] S. Xie, T. Li, Z. Xu, Y. Wang, X. Liu, and W. Guo, "A high-response transparent heater based on a CuS nanosheet film with superior mechanical flexibility and chemical stability," *R. Soc. Chem.*, pp. 6531–6538, 2018.

[2] M. Bobinger *et al.*, "Solution-Processing of Copper Nanowires for Transparent Heaters and Thermo-Acoustic Loudspeakers," *IEEE Trans. Nanotechnol.*, vol. 17, no. 5, pp. 940–947, 2018.

[3] D. Lee, G. Bang, M. Byun, and Choi Dooho, "Highly flexible , transparent and conductive ultrathin silver film heaters for wearable electronics applications," *Thin Solid Films*, no. January, pp. 1–6, 2020.

[4] R. Gupta, K. D. M. Rao, S. Kiruthika, and G. U. Kulkarni, "Visibly Transparent Heaters," *ACS Appl. Mater. Interfaces*, vol. 8, no. 20, pp. 12559–12575, 2016.

[5] G. Liu *et al.*, "Comprehensive Stability Improvement of Silver Nanowire Networks via Self-Assembled Mercapto Inhibitors," *ACS Appl. Mater. Interfaces*, 2018.

[6] Y. Zhu, Y. Deng, P. Yi, L. Peng, X. Lai, and Z. Lin, "Flexible Transparent Electrodes Based on Silver Nanowires: Material Synthesis, Fabrication, Performance, and Applications," *Adv. Mater. Technol.*, vol. 4, no. 10, pp. 1–22, 2019.

[7] E. J. Lee, Y. H. Kim, D. K. Hwang, W. K. Choi, and J. Y. Kim, "Synthesis and optoelectronic characteristics of 20 nm diameter silver nanowires for highly transparent electrode films," *RSC Adv.*, vol. 6, no. 14, pp. 11702–11710, 2016.

[8] P. Zhang *et al.*, "Silver nanowires: Synthesis technologies, growth mechanism and multifunctional applications," *Mater. Sci. Eng. B Solid-State Mater. Adv. Technol.*, vol. 223, pp. 1–23, 2017.

[9] K. M. S. K. Praveen, A. Kumar, S. John, and H. C. Barshilia, "Synthesis of high yield silver nanowires for transparent flexible conductor applications," *Mater. Today Proc.*, vol. 5, no. 4, pp. 10883–10888, 2018.

[10] Y. Shi *et al.*, "Synthesis and applications of silver nanowires for transparent conductive films," *Micromachines*, vol. 10, no. 5, 2019.

[11] H. Wang, Y. Wang, and X. Chen, "Synthesis of uniform silver nanowires from AgCl seeds for transparent conductive films via spin-coating at variable spin-speed," *Colloids Surfaces A Physicochem. Eng. Asp.*, vol. 565, no. November 2018, pp. 154–161, 2019.

[12] M. Shaban, G. F. Attia, M. A. Basyooni, and H. Hamdy, "Synthesis and characterization of Tin oxide thin film, effect of annealing on multilayer film," *J. Mod. Trends Phys. R*, vol. 14, no. January, pp. 90–99, 2014.

[13] M. Singh, H. M. Haverinen, P. Dhagat, and G. E. Jabbour, "Inkjet printing-process and its applications," *Adv. Mater.*, vol. 22, no. 6, pp. 673–685, 2010.

[14] H. Koga, M. Nogi, N. Komoda, T. T. Nge, T. Sugahara, and K. Suganuma, "Uniformly connected conductive networks on cellulose nanofiber paper for

transparent paper electronics," *NPG Asia Mater.*, vol. 6, no. 3, pp. 1–8, 2014.

[15] K. J. Brobbey *et al.*, "One-step flame synthesis of silver nanoparticles for roll-to-roll production of antibacterial paper," *Appl. Surf. Sci.*, vol. 420, pp. 558–565, 2017.

[16] S. Cataldo and B. Pignataro, *Polymeric thin films for organic electronics: Properties and adaptive structures*, vol. 6, no. 3. 2013.

[17] M. Veeramanikandan, T. V. Arjunan, and P. Jidhesh, "Experimental investigation of sandwich glazed solar photovoltaic Module," *Mater. Today Proc.*, vol. 27, pp. 136–139, 2019.

[18] A. El Amrani, A. Mahrane, F. Y. Moussa, and Y. Boukennous, "Solar module fabrication," *Int. J. Photoenergy*, vol. 2007, no. June 2014, 2007.

[19] M. Schregel, "Silver nanowire networks as transparent electrodes," Gelsenkirchen, 2014.

[20] S. M. Bergin, Y. H. Chen, A. R. Rathmell, P. Charbonneau, Z. Y. Li, and B. J. Wiley, "The effect of nanowire length and diameter on the properties of transparent, conducting nanowire films," *Nanoscale*, vol. 4, no. 6, pp. 1996–2004, 2012.

[21] X. Y. Zeng, Q. K. Zhang, R. M. Yu, and C. Z. Lu, "A new transparent conductor: Silver nanowire film buried at the surface of a transparent polymer," *Adv. Mater.*, vol. 22, no. 40, pp. 4484–4488, 2010.

[22] R. M. Mutiso, M. C. Sherrott, A. R. Rathmell, B. J. Wiley, and K. I. Winey, "Integrating simulations and experiments to predict sheet resistance and optical transmittance in nanowire films for transparent conductors," *ACS Nano*, vol. 7, no. 9, pp. 7654–7663, 2013.